Area-Averaged Surface Fluxes in a Semiarid Region with Partly Irrigated Land: Lessons Learned from EFEDA

M. ANNA OSANN JOCHUM

ALFAclima Asesoramiento Medioambiental, Albacete, Spain, and Wageningen University, Wageningen, Netherlands

HENDRIK A. R. DE BRUIN AND ALBERT A. M. HOLTSLAG

Wageningen University, Wageningen, Netherlands

ALFONSO CALERA BELMONTE

Universidad de Castilla-La Mancha, Albacete, Spain

(Manuscript received 9 July 2004, in final form 4 October 2005)

ABSTRACT

The European Field Experiment in a Desertification-Threatened Area (EFEDA) provides a comprehensive land surface dataset for a semiarid Mediterranean environment with natural vegetation and cultivated dry and irrigated land. This paper discusses the methods and practical aspects of deriving area-averaged fluxes for a range of areas from the whole EFEDA region to several numerical weather prediction model grid cells (on 10–100-km scales). A time series of grid-scale surface fluxes for the entire observational period of 1 month was obtained from weighted surface averages, using a crop phenology–based land use classification together with a homogenized set of surface observations representative of the four major vegetation classes. The flux-aggregated surface observations were compared with two other approaches to obtain grid-scale fluxes (airborne flux observations and radiosondes in conjunction with a simple mixed-layer model). The area-aggregated fluxes (in particular of latent heat) depend strongly on the location of the area boundaries whenever a significant fraction of irrigated land is present. This result confirms clearly the importance of adequately accounting for tiles of irrigated land in surface schemes and corresponding physiographic databases of large-scale models. A simple way to accommodate for minimum information on the canopy water status is proposed in terms of the distinction of at least two seasonal classes of irrigated crops—one of spring and one of summer growing cycles. The main lesson from this aggregation exercise concerns the role of irrigation. First, this study quantifies the uncertainties in the space–time pattern and its effects on aggregated surface fluxes for the first time on the grounds of observational data. Second, it demonstrates practical ways to accomplish the parameterization of irrigation in flux aggregation schemes, by identifying the key data along with their possible sources and by defining a practical implementation procedure.

1. Introduction

One of the objectives of the European Field Experiment in a Desertification-Threatened Area (EFEDA; Bolle et al. 1993) was to obtain a consolidated dataset of area-averaged surface fluxes for the duration of the field experiment and for the scale of the entire area. Surface fluxes at the grid scale are needed for the evaluation of turbulent transport parameterizations in large-scale numerical models (Beljaars and Holtslag 1991). However, they are not immediately obtained from any kind of observations. Different methods are often combined to achieve this goal.

Surface observations provide continuous time series of observational grid-scale fluxes through weighted averaging. Notwithstanding, each surface station "sees" only its limited fetch area (or source area; Schmid 1994). The question is how representative a weighted tower average is, and if any adjustments are necessary

Corresponding author address: Dr. M. Anna Osann Jochum, ALFAclima Asesoramiento Medioambiental, Avenida de España, 9, E-02002 Albacete, Spain.
E-mail: ajochum@terra.es

(for strata, processes, and/or scales not covered). Comparison with other approaches helps to answer these questions. Airborne flux observations provide an area-wide view at single points in time on single days. Thus they offer independent reference values for comparison, often around local noon and on fair-weather days. Radiosondes provide another alternative areal perspective. In conjunction with a simple mixed-layer (ML) model framework, they can provide semiobservational continuous regional fluxes during daytime.

André et al. (1990) were the first to compare regional flux approaches using data from Hydrologic Atmospheric Pilot Experiment-Modélisation du Bilan Hydrique (HAPEX-MOBILHY; André et al. 1988). Holtslag and Ek (1996) use the same dataset in comparison with a one-dimensional coupled land surface and atmospheric boundary layer model to investigate regional fluxes at the 10-km scale. Gottschalk et al. (1999) compare grid-scale fluxes for Northern Hemisphere Climate Processes Land Surface Experiment (NOPEX; Halldin et al. 1999). Grunwald et al. (1996, 1998) compare weighted surface observation averages and airborne flux estimates for two subareas of the EFEDA region (squares of 10–30-km sides). Bastiaanssen et al. (1997) derive area-aggregated surface fluxes from remote sensing and compare with EFEDA surface observations. More recent examples in this nonexhaustive list include Observations at Several Interacting Scales (OASIS; Leuning et al. 2004) and Lindenberg Inhomogeneous Terrain–Fluxes between Atmosphere and Surface: A Long-Term Study (LITFASS; Beyrich et al. 2002). These studies have all in common the case study view.

Mahrt et al. (2001) start from a different perspective, pursuing the objective of delivering time series of observational aggregates for an entire season. They discuss a number of practical solutions to problems they find on the way to calculating area-averaged fluxes over the Boreal Ecosystem–Atmosphere Study (BOREAS; Sellers et al. 1997) area based on a combination of tower and aircraft observations. One of their main conclusions is the need to adjust the weighted surface averages by means of aircraft-derived Bowen ratios.

The objective of this work is along similar lines, aiming at generating a 1-month time series of regional fluxes for the EFEDA semiarid environment. Irrigation is the prominent feature here, with its marked influence on the surface energy budget. Several numerical modeling studies concluded that irrigated areas have a strong influence on regional fluxes (Adegoke et al. 2003; de Rosnay et al. 2003; Zaitchik et al. 2005). We investigate here the irrigation patterns and their impact on regional fluxes for the first time on the grounds of observational data.

Weighted surface observations are the only possible way to generate time series of regional fluxes. The contribution of aircraft and other intensive short-term observations helps one to decide on potentially necessary adjustments to these values on the basis of case study comparisons. The individual approaches are discussed here on the grounds of the available data, and grid-element fluxes on a scale range of 10–100 km are derived.

The concept of scale aggregation plays a role in several of these steps. The relevant definitions are briefly recalled here. A grid-scale flux or an area-averaged flux is simply the mean flux across a given area (or grid element of a numerical model). Parameter aggregation is defined as the "spatial averaging of heterogeneous surface variables to obtain effective values which are representative of the area" (Michaud and Shuttleworth 1997). Flux aggregation refers to the spatial averaging of the patch-scale fluxes.

The observations are described in section 2. Flux aggregation through weighted surface averages is the topic of section 3. Details of the irrigation aspects are discussed in section 4. Section 5 is dedicated to the regional flux estimation from aircraft and from radiosondes in an ML slab model framework. The synthesis of the results from all relevant methods is discussed in section 6; the conclusions are summarized in section 7.

2. The observations

The general rationale of EFEDA (Bolle et al. 1993) followed along the lines of the early land surface experiments (Jochum et al. 2000). Its goal was to document the land surface state and processes in a large-scale model grid cell volume as densely as needed for the specific area and during a limited time period. The observational strategy consisted of simultaneous measurements at three heavily instrumented intensive study areas ("supersites"), with instrumented aircraft and satellite remote sensing providing the observational link between these sites.

a. Experimental site

The EFEDA regional area was selected to represent a model grid cell located in a dry climate (350-mm mean annual precipitation), with land uses ranging from natural vegetation to dry and irrigated agricultural lands, as typically encountered in all Mediterranean countries. The observational period covered the entire month of June in 1991. June is the month with the most actively growing irrigated crops in the area, and it co-

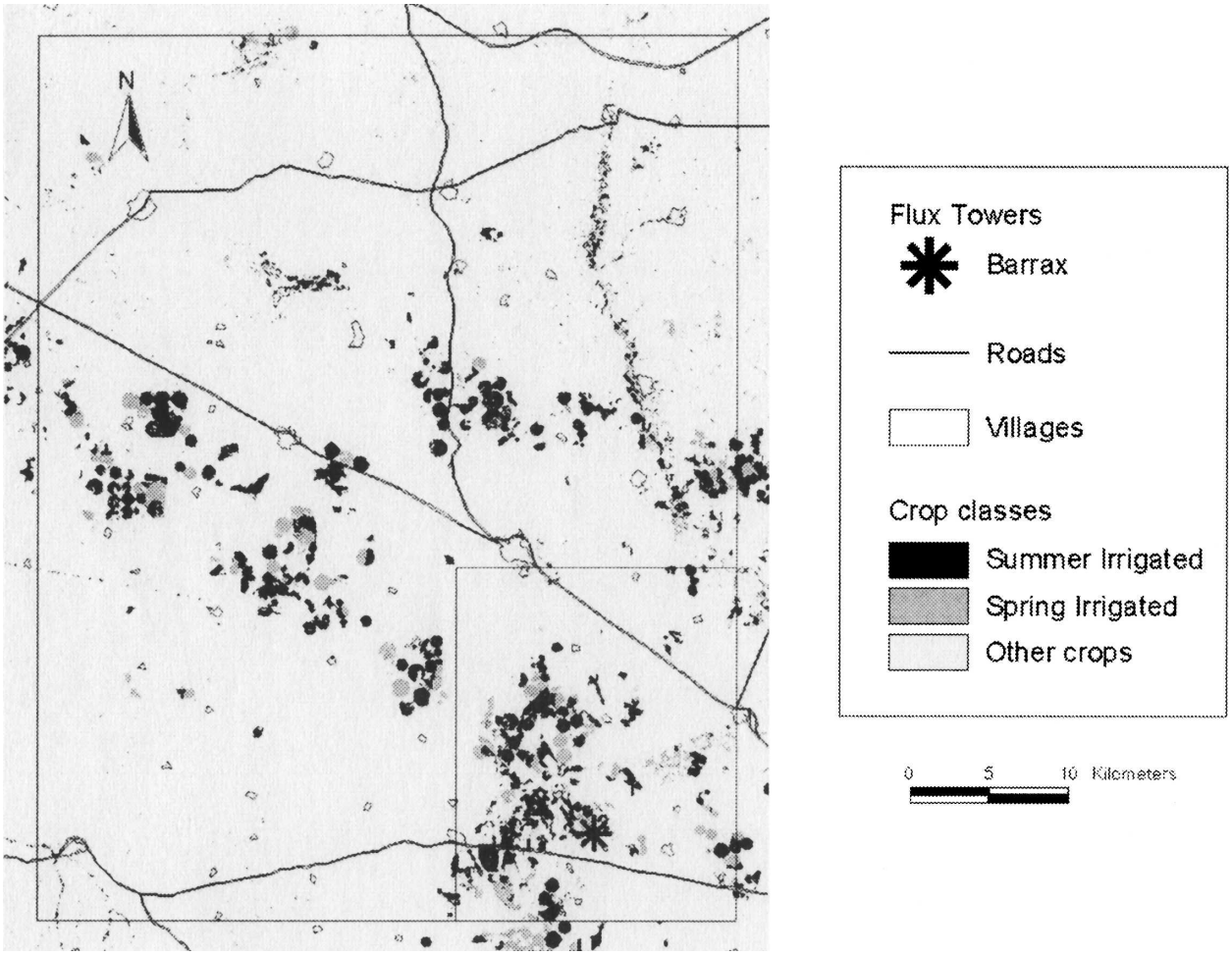

FIG. 1. Distribution of irrigated fields (shaded areas) in the eastern part of the EFEDA region, with supersite Barrax (asterisk) based on the 1991 land use classification of Calera Belmonte (2000). The rectangles represent grid cells of HIRLAM 0.5° and 0.2°, respectively (see Table 6 for coordinates).

incides with the major dry-down after the spring rainfall.

The EFEDA region is located in La Mancha, part of the Castilian high plateau in the southeast of Spain, at an average elevation of 700 m above mean sea level. It extends about 60 km in the north–south direction and 80 km in the east–west direction. The area is generally flat, with elevation variations up to 100 m, but is surrounded and influenced by mountain ranges at a 35–45-km distance from three directions.

The Tomelloso supersite represents nonirrigated agricultural land. The site forms part of the largest vine-growing area in the world. The Barrax supersite is located above several subterranean aquifers, which are exploited for irrigation purposes. The irrigated fields are distributed very unevenly (Fig. 1). The dominant dry farming is dedicated to winter cereals. The Rada de Haro supersite is located in a mountainous area at a mean altitude of 810 m above sea level where agricultural activity is marginal. Together, these supersites represent the major land use classes of the area that are relevant in June: natural vegetation (Rada de Haro), dry summer crops (Tomelloso), irrigated summer crops, and fallow land (both at Barrax).

b. Measurements and data

A total of 21 surface flux stations of different configurations was deployed by 10 groups, some operating only during part of the EFEDA period (Bolle et al. 1993). The major concentration (13 stations) was found in the Tomelloso supersite, along with the most complete temporal coverage of the entire month of June 1991. Less spatial and temporal coverage was dedicated to the other two supersites, where each major vegetation class (including bare soil) was monitored by one or two flux stations.

Linder et al. (1996) have derived representative, standardized datasets for the four major vegetation classes for the purpose of intercomparing surface schemes. Their datasets consist of atmospheric forcing data, general soil and vegetation data (input needed to run the schemes), and flux data for comparison. Table 1 summarizes the datasets and gives a list of parameters. The datasets cover 27 (Tomelloso: vine), 26 (Barrax: irrigated maize), 11 (Barrax: bare soil), and 5 + 8 (Rada de Haro: natural vegetation) days.

De Bruin et al. (1993) performed a detailed assessment of the observational errors of the surface energy balance components as measured by the individual flux stations. They find a 7% error of net radiation and a 30% error of soil heat flux for all methods. The heat and moisture flux errors vary widely according to the methods used (eddy correlation, profile method, Bowen ratio, or temperature variance). While sensible heat flux errors remain below 20%, the moisture fluxes are affected by large uncertainties of up to 72%. Because of the large scatter (and inherent difficulties of measuring moisture flux in very dry conditions), the latent heat flux was recalculated by Linder et al. (1996) for all stations as the residual in the energy balance equation.

Airborne flux observations were performed by two aircraft during the second half of June 1991. Data from the Deutschen Zentrum für Luft- und Raumfahrt (DLR) (German Aerospace Center) Falcon 20 are used here. The aircraft carried instrumentation to measure and derive basic meteorological parameters (temperature, humidity, pressure, and wind), turbulent fluxes (heat, moisture, and momentum), the four radiation flux components, water vapor and aerosol backscatter vertical profiles, and video images of the ground. Jochum (1993b) and Michels and Jochum (1995) describe the instrumentation, flight patterns, and analysis details. With high-resolution (100 Hz) sensors and sampling and at a typical low-level true airspeed of 135 m s^{-1}, scales down to 15 m are captured. The individual time series for each flight track ("leg") are detrended and high-pass-filtered before fluxes and other turbulence statistics are computed. A cutoff wavelength of 20 km was used for all legs longer than 60 km. This ensures that long-wavelength contributions to the turbulent fluxes are retained. Kinematic fluxes are computed by means of the eddy covariance method and converted to energy fluxes using the measured mean air density.

Radiosondes were launched daily (on some days hourly) at the Tomelloso and Barrax supersites. At Tomelloso, Météo France operated an Omega navigation system in conjunction with Vaisala RS80 sondes. At Barrax, the University of Karlsruhe used a Plessey WF33 radar-tracking system together with Graw TDFS87 sondes. The accuracy of both systems is estimated as 0.5 g kg^{-1} for humidity and 0.5 K for temperature. The vertical resolution is 30–50 m, except for wind observations using the Omega system (150–300 m).

c. *Synoptic situation*

The synoptic situation during the observational period of 1–30 June 1991 was mostly characterized by anticyclonic conditions. The only major perturbation occurred in the first 3 days, when strong convective activity produced some precipitation in the EFEDA region. During the rest of the month, a small number of weak frontal systems passed over Spain. They affected the EFEDA region on 5 days, mostly associated with increased cloudiness.

This synoptic situation offers a natural classification of the experimental days into the two broad categories of "anticyclonic" and "slightly unstationary" conditions, excluding the first 3 days. The anticyclonic cases

TABLE 1. Contents of consolidated surface datasets of Linder et al. (1996). Here SW = shortwave radiation and LW = longwave radiation. Each column is a separate list; there is no correspondence among columns.

Atmospheric forcing data (half-hourly values)	Surface flux data (half-hourly values)	Vegetation and soil data
Air temperature at 2 m	Sensible heat flux	Roughness lengths (momentum, heat)
Relative humidity at 2 m	Latent heat flux	Emissivity and albedo
Wind speed at 10 m	Soil heat flux	Vegetation fraction
Air pressure	Net radiation	Leaf area index
Incoming SW radiation	Friction velocity	Minimum stomatal resistance
Outgoing SW radiation	Radiative surface temperature	Soil texture
Incoming LW radiation		Saturation, field capacity, and wilting-point water content
Precipitation		Thermal conductivity
		Saturated hydraulic conductivity and head
		Soil depth
		Root density profile
		Initial profiles of soil temperature and moisture

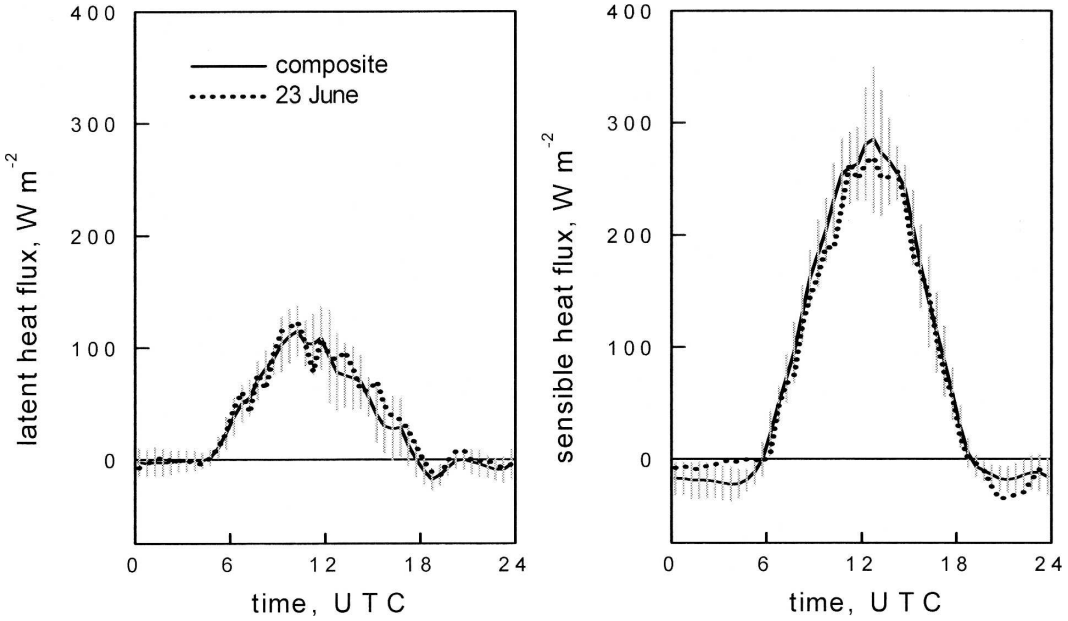

FIG. 2. Diurnal cycle of (left) latent and (right) sensible heat flux at Tomelloso (vine). Composite of all (22) anticyclonic days (solid line) and 23 Jun (dotted line). Error bars indicate standard deviation of the mean.

represent a large sample (22 days) of fairly homogeneous conditions that is well covered by surface observations and at least one to two daily radiosoundings. The second half of June 1991 (with its added datasets from aircraft and more frequent radiosoundings) holds eight of these cases, with 23 June most densely covered by observations.

Figure 2 shows an example of the variability across the anticyclonic sample. The sensible heat flux varies by less than 23%, while latent heat flux variability is highest (up to 43%). The variability of net radiation (not shown) is small (less than 14%) and apparently related to differences in cloud cover in the early afternoon. The observations on 23 June (dotted lines) are almost identical to the composite (solid lines). The situation is very similar for the other two dry vegetation classes (Rada de Haro: natural, and Barrax: bare), while the irrigated vegetation (Barrax) needs special treatment (see section 3) because of the irregular irrigation timing.

3. Aggregation of surface flux observations

This section describes the process of aggregating the local-scale surface observations to the regional scale. The regional flux F (soil, sensible, or latent heat flux or net radiation) is here obtained through flux aggregation in a straightforward manner by weighted averaging of the fluxes f_i observed in each vegetation class i. The weights are taken as the fractional contributions a_i of each vegetation class to a given area,

$$F = \sum_{i=1}^{N} a_i f_i, \quad \text{where} \quad \sum_{i=1}^{N} a_i = 1. \tag{1}$$

The cornerstone of any such flux aggregation is an adequate land use classification that properly identifies and differentiates the most contrasting surface types. Pelgrum and Bastiaanssen (1996) have shown that different classifications produce different area aggregates.

Equation (1) is used here with four land use classes ($i = 4$) from the Calera Belmonte (2000) classification. The weights a_i are derived from the same classification. The per-class fluxes f_i are taken from the flux tower observations as consolidated from the Linder et al. (1996) dataset. The irrigated-class fluxes are obtained from normalizing the Barrax-irrigated flux tower in a way that parameterizes the irregular time–space pattern of irrigation. This normalizing approach is explained in section 4, and details of the aggregation procedure are described in the rest of this section.

a. Seasonality of evapotranspiration

We argue here that it is vital in this kind of Mediterranean environment to use a land cover classification based on local/regional vegetation phenological cycles. It is these cycles that largely determine the actual evapotranspiration (ET) of the individual fields, and thus their surface energy budget (SEB). In the semiarid climatic conditions of the EFEDA region, ET is primarily limited by water availability rather than by the

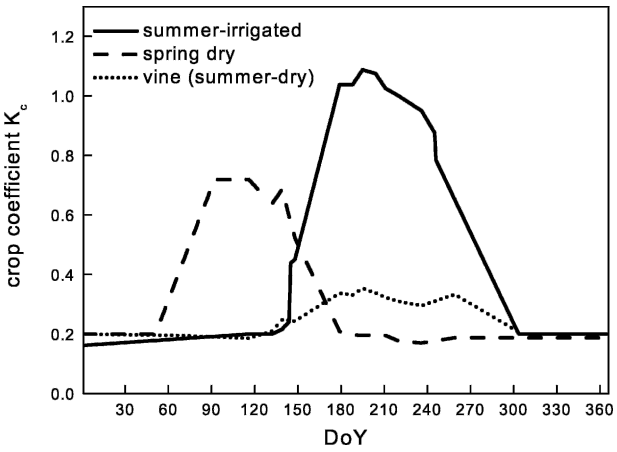

FIG. 3. Crop phenological cycles of major crop classes in the EFEDA region (from González-Piqueras 2006).

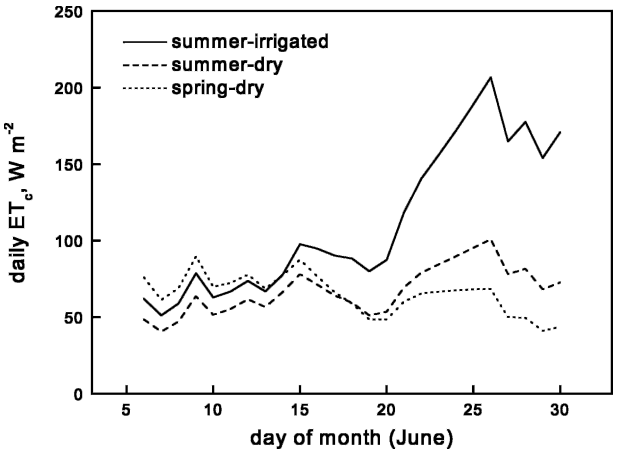

FIG. 4. Crop evapotranspiration ET_c of summer-irrigated and spring- and summer-dry crop classes in the 1991 EFEDA region.

available energy or processes determining vertical water vapor transfer.

Figure 3 serves to illustrate this highly seasonal nature of ET for the main relevant vegetation classes (spring irrigated, summer irrigated, summer dry, natural) in the EFEDA region. The ET concepts and definitions are used here according to Allen et al. (1998). Reference evapotranspiration ET_0 is the ET rate of a reference surface (a hypothetical grass surface with an assumed crop height of 0.12 m, a fixed surface resistance of 70 s m^{-1}, and an albedo of 0.23). Crop evapotranspiration ET_c is similarly defined for a nongrass crop under standard conditions (well watered, disease free, grown in large fields),

$$ET_c = K_c ET_0. \quad (2)$$

The crop coefficient K_c is introduced to express the differences between a given crop and the reference grass and is defined as the ratio of ET_c over ET_0. Figure 3 shows the temporal evolution of the crop coefficient K_c [based on data of González-Piqueras (2006) and Calera Belmonte (2000)]. Because of late-winter frost and very dry conditions, the seasonal cycles of most crops were late in 1991. The ET_0 was calculated hourly and daily from an agrometeorological station on a standard grass surface, using the Penman equation adapted to the area, and K_c was determined weekly by extensive field work in all major crops [see Montoro et al. (2004) for all details]. Figure 4 shows daily ET_c for 1991 for the crops of main interest. Weekly per-crop ET_c is very often used as a measure of irrigation requirements (Allen et al. 1998) and determines water applied by farmers, so it gives a rough approximation of actual ET in irrigated fields (Montoro et al. 2004). Because of the combined effect of high ET_0 during the summer and the fully mature crop growth stage (maximum values of K_c) in July–August, the summer-irrigated class is the one that needs the most attention here.

b. Land use classification

The Landsat remote sensing–based multitemporal classification of Calera Belmonte (2000) was selected for its simplicity and functionality. The vegetation classes are defined according to the different phenological growth cycles of the individual crops (Martínez and Calera 2001). Table 2 gives the definition of the classes and adds the relevant information on the crop phenological status for June 1991. In the EFEDA region, the spring crops (dry and irrigated) have either been harvested or are senescent by mid-June. Therefore, their SEB is similar to that of bare soil or fallow land, and there is no need to represent these classes separately in the surface flux aggregation. The forest class occupies a very small area fraction and is regrouped into the natural vegetation class (which has similar characteristics). The remaining four classes perfectly match the vegetation types covered by the EFEDA observations. Tomelloso corresponds to "summer dry," Rada de Haro to "natural," Barrax bare to "bare," and Barrax irrigated to "summer irrigated." Thus the Calera Belmonte (2000) land use classes can be remapped onto these four classes, for which there are complete SEB observations available during June of 1991.

c. Surface energy budget of different vegetation classes

The diurnal cycles of the SEB of the three dry land use classes are similar to each other (SUM-dry, BARE,

TABLE 2. Definition of vegetation classes in Calera Belmonte (2000) and range of relevant crop parameters for June 1991. Italics indicate continuous change from beginning to end of month; boldface indicates rapid change in early June. Soil moisture ranges are from Allen et al. (1998); albedo is from Linder et al. (1996).

	BARE	SPR-dry	SPR-irrig	SUM-dry	SUM-irrig	NAT	FOR
Description	Bare and fallow	Spring dry crop	Spring irrigated	Summer dry crop	Summer irrigated	Natural vegetation	Forest
Albedo	0.23–0.28	0.23–0.28	0.23–0.28	0.28	0.15–0.25	0.2	0.2
Vegetation height (m)	0	**1 → 0**	**1 → 0**	0.6	*0.2 → 1.5*	1	3
Fraction of vegetation	0	**0.6 → 0**	**0.8 → 0.1**	0.1	*0.1 → 0.8*	0.15	0.30
Leaf area index	0	**0.3 → 0**	**0.4 → 0.1**	*0.1 → 0.4*	*0.2 → 0.4*	0.5	1
Soil texture class	Sandy–clay–loam (15%–25% clay, 60%–75% sand)					Sand (<10% clay, >85% sand)	
Field capacity volume moisture content	0.18–0.28 $m^3\ m^{-3}$					0.07–0.17 $m^3\ m^{-3}$	
Wilting-point volume moisture content	0.06–0.16 $m^3\ m^{-3}$					0.02–0.07 $m^3\ m^{-3}$	

and NAT in Fig. 5, showing the example of 23 June). Intersite variations are within the range of within-site variability and flux observation uncertainties (de Bruin et al. 1993 and section 2). Day-to-day variations in dry vegetation classes are also small (see Fig. 2). The most notable influence on the SEB comes from irrigation (SUM-irrig in Fig. 5), which is not performed in any continuous way across all fields and at all times (see section 4). Figure 5a shows the peak irrigation-influenced SEB of 23 June (the day immediately following nighttime irrigation).

Before entering in the details of irrigation schedul-

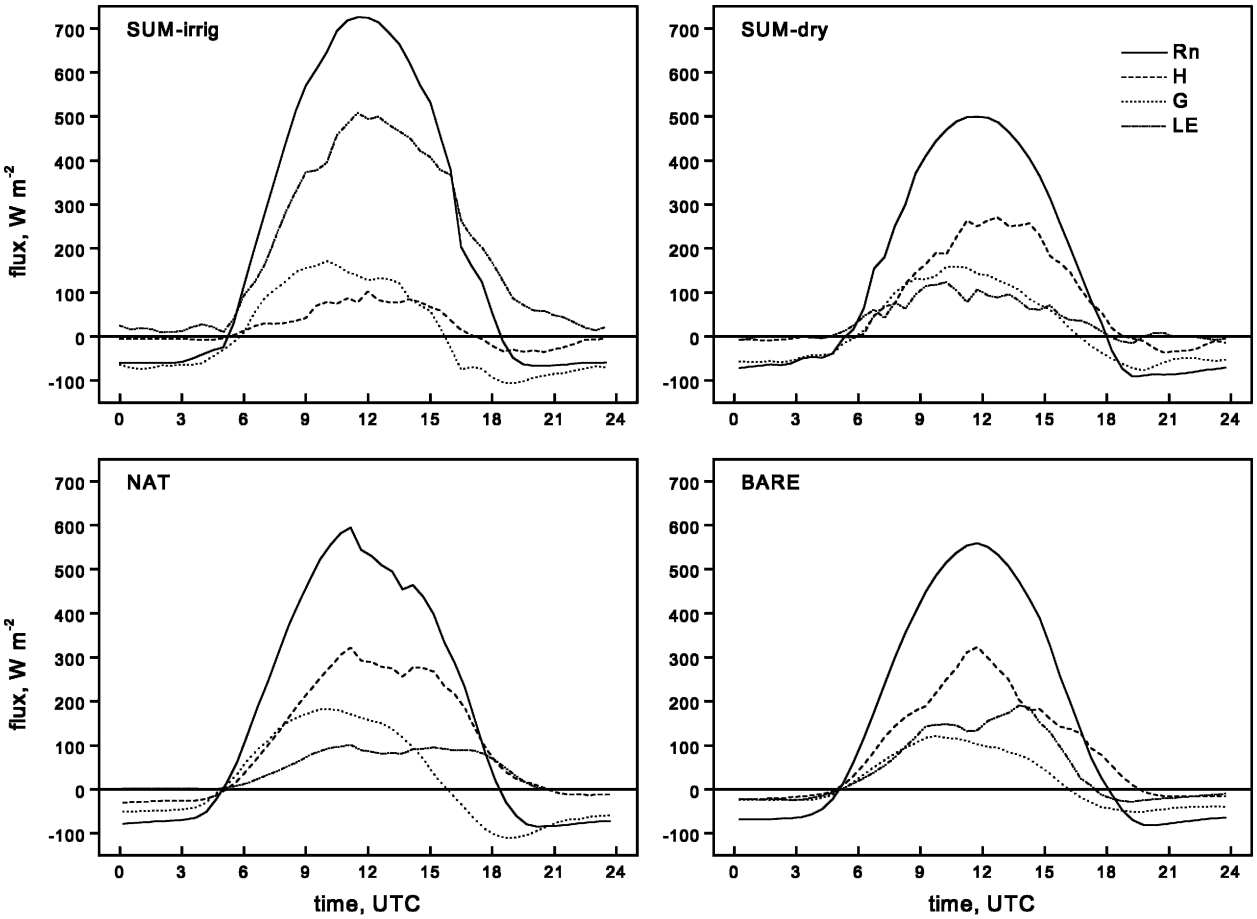

FIG. 5. Surface energy budget on 23 Jun for each vegetation class: (top left) summer-irrigated crops (SUM-irrig), (top right) summer-dry crops (SUM-dry), (bottom left) natural vegetation (NAT), and (bottom right) bare soil (BARE).

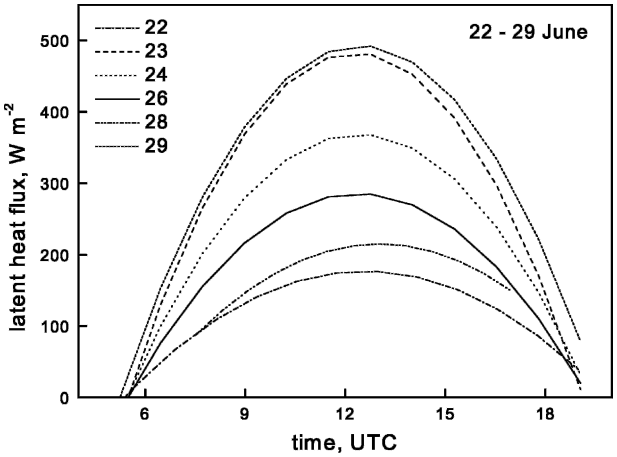

FIG. 6. Diurnal cycle of latent heat flux (W m^{-2}) at irrigated maize flux station from 22 to 29 Jun. Irrigation took place during the nights of 22/23 and 28/29 Jun (2200–0030 UTC).

ing, its effect on the local SEB is illustrated here by means of an 8-day sequence (22–29 June) (see also Grunwald et al. 1996). These observations were performed in a center pivot planted with maize, which was irrigated during the nights of 22/23 and 28/29 June. Irrigation of the sector where the mast was located took place from 2200 to 0030 UTC on either occasion.

Figure 6 shows the diurnal cycle of the latent heat flux during this 8-day sequence. The same sequence for the dry field reference (not shown) does not exhibit significant variations over the 8 days. The irrigated field SEB shows clearly the big differences induced by the irrigation on the second day and the very gradual relaxation into a drier ("irrigation off") mode. The effect is visible from the moment when irrigation starts (in other sectors of the pivot) in the late afternoon of the first day. The most notable difference is in the latent heat flux (Fig. 6), which reaches values of 490 W m^{-2} instead of 170 W m^{-2} toward the end of the irrigation cycle. The sensible heat flux is reduced accordingly (shown only for 23 June, see Fig. 5a). The overall available energy (through the net radiation) is increased on the irrigation day, because both the albedo and the surface temperature are reduced during the period of high water availability. One day after irrigation, the latent and sensible heat fluxes are still close to their wet extremes. Around the fifth or sixth day, the SEB is normally back to a state of minimum water availability and on the sixth or seventh day the irrigation cycle starts again.

4. Effect of irrigation in flux aggregation

Given the observed large differences in SEB of the irrigated fields, the area-aggregated fluxes (in particular of latent heat) will depend strongly on the location of the area boundaries, whenever a significant fraction of irrigated land is present. The scale dependence of this effect can be estimated in a simple way by relating scale to the areal fraction of irrigated land in any given domain. Figure 7 illustrates the situation for latent and sensible heat flux on 23 June with areal fractions of 10% and 30%, respectively. The peak aggregated latent heat flux (right panel) ranges from 133 to 213 W m^{-2}. In other words, raising the irrigated area fraction from 10% to 30% results in an enhancement of the peak aggregated moisture flux by 60%. At the same time, the peak aggregated sensible heat flux (left panel) is reduced by about 15% (from 242 to 202 W m^{-2}). This confirms qualitatively and quantitatively the model-based findings of Adegoke et al. (2003), Zaitchik et al. (2005), and Haddeland et al. (2006).

a. Irrigation patterns and practice

The spatial pattern of irrigation in the EFEDA region is determined by the fact that groundwater is the major water source. This leads to a highly irregular spatial distribution of irrigated fields over a wide area (rather than being concentrated near a river-based water source), with scales of individual fields (about 1 km) being generally smaller than ABL scales (3 km). The spatial pattern of irrigated fields across the area (including a detailed crop inventory) in 1991 is known with high accuracy from the intensively validated classification of Calera Belmonte (2000). A small error (about 3%) in the delimitation of the irrigated area is introduced by the effect of the spatial resolution of the Landsat images and their half-pixel georeferencing accuracy (Martínez and Calera 2001).

The temporal pattern results from an overlay of three cycles plus the day-to-day decisions of farmers. The annual cycle of ET_0 is well known through measurements at the agrometeorological stations. The seasonal phenological growth cycle of each crop is well known from intensive fieldwork (Montoro et al. 2004). It ranges from 4 weeks (alfalfa) to 6 months (vine), with the major concentration of irrigation events during the active crop-growing phase (steep ascent in K_c curves, see Fig. 3). The Irrigation Advisory Service (IAS) introduces a (technical) weekly cycle through their irrigation scheduling recommendations (Montoro et al. 2004). Therein, weekly ET_c is calculated each week for the previous week and a prediction is derived for the coming week, which are both communicated to the farmers by media, telephone, or Internet.

Based on the weekly recommended ET_c, farmers would make their own decisions on the actual water

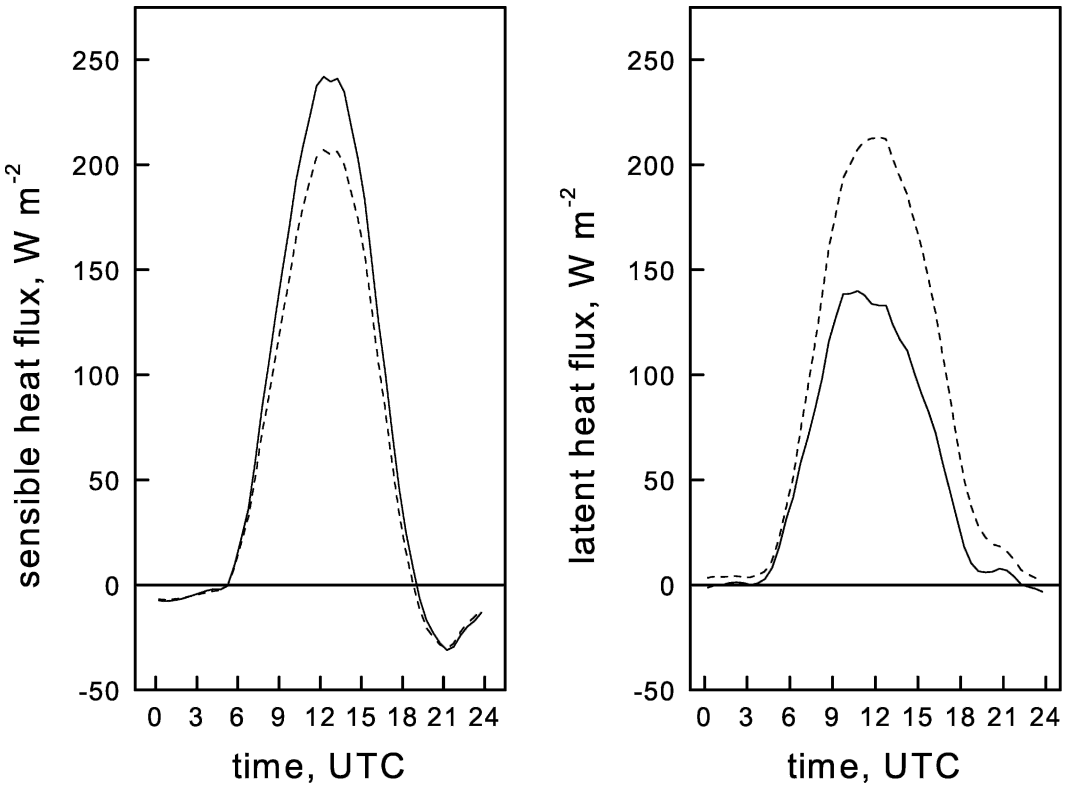

FIG. 7. Area-aggregated surface (left) sensible and (right) latent heat fluxes for different area fractions of irrigated fields (solid line: 10%; dashed line: 30%).

quantity application and the irrigation timing in each of their fields. For example, during June of 1991, there were four irrigation events in the particular field where the flux tower was located. In the other fields within the summer-irrigated crop class, these events possibly took place on other dates. The farmers' day-to-day decisions introduce a twofold uncertainty (which also varies from week to week)—first, whether they follow the IAS recommendations, and second, which day(s) in the week they would actually irrigate a given field. The farmers' "probable behavior" was to irrigate according to ET_c, but the uncertainty on daily scales remains.

b. Uncertainty scenarios

Four scenarios were used to estimate the uncertainty introduced in surface flux aggregation by the irregular irrigation timing. The full 1-month time series of 24-h mean surface fluxes was analyzed for the purpose of defining the scenarios (Table 3). Figure 8 shows this time series for latent heat flux (where the major effects are found) at the Barrax-irrigated and Tomelloso flux stations. The first shows clearly the irrigation peaks on the days after each irrigation night and the gradual relaxation during the subsequent days, as observed in the diurnal cycles of Fig. 6. It also shows the general agreement with ET_c (Fig. 4). In contrast, the Tomelloso daily time series is fairly smooth, with daily ET slowly increasing with rising air temperature and solar radiation during June.

Figure 9 shows the time series of 24-h means of latent heat flux aggregated according to the different scenarios, using a 40% areal fraction of irrigated land as an example. Except for "irrigation on" days, the difference between scenarios is small during the initial third of June, when the irrigated maize was in incipient growth stage (small fractional area covered, low height), with evaporation outweighing transpiration. It is larger (up to 20%) toward the end of June, when almost full canopy cover is reached and most of ET comes from transpiration.

c. Practical treatment of irrigation cycles

A practical flux aggregation should be simple and yet as realistic as possible (i.e., corresponding to the farmers' habits of maintaining their fields close to ET_c). The "wet limit" scenario is one acceptable option. It has the disadvantage that the concept of daily (or even weekly) ET_c implies loosing the diurnal cycle dynamics of the

TABLE 3. Definition of scenarios for irrigation cycle timing effects on regional fluxes.

Scenario	Name	Definition
Scenario I	Dry limit	The 24-h mean latent heat flux is taken from a second-order polynomial fit to the Barrax graph in Fig. 8 (i.e., interpolating the "low" days in the irrigation cycle). A simplified approximation consists of using the daily flux observed in dry vegetation (Tomelloso, which agrees with low days in the irrigation cycle at the beginning of June and is substantially below low days in later stages of crop growth).
Scenario II	Wet limit	Calculation is from daily ET_c of maize. This corresponds to irrigation water applied by farmers according to the crop water requirements provided by the IAS ("probable behavior of farmers").
Scenario III	Homogeneous	It is assumed that the irrigation peaks are distributed homogeneously across the area and the time of the weekly irrigation cycle (i.e., one-seventh of all fields are irrigated on each day of the week).
Scenario IV	In tune	It is assumed that all fields are irrigated in tune with the experimental field. This means that the Barrax-irrigated flux station observations are directly used as f_i in the flux aggregation scheme.

flux data. For this reason, the fourth scenario, "in tune with flux station," was introduced. However, the single-day irrigation peaks are not fully smoothed out by the aggregation. To adjust the area aggregate for these peaks (which do not occur everywhere on the same day), while maintaining the direct use of the Barrax-irrigated flux station, a normalization procedure was developed. It scales each flux observation f_i with the ratio of ET_c over the corresponding 24-h mean flux. The resulting aggregated flux is close to the wet limit values everywhere. Therefore, this parameterization approach is adopted here to derive the regional fluxes.

During the 1991 growing season, maize was planted in 95% of the irrigated area (Calera Belmonte 2000). Other irrigated crops, such as vegetables, do not reach full canopy cover, and so their crop coefficient and resulting ET_c are somewhat lower than those of maize. To account for their presence, the Barrax station–derived latent heat fluxes are reduced by 5% before entering the flux aggregation algorithm.

5. Grid-scale fluxes from other methods

a. Area-averaged fluxes from aircraft observations

Flux aircraft offer two main alternatives to obtain regional fluxes. The first approach is analogous to the flux aggregation of surface observations by means of weighted averaging. It requires a very low flying aircraft that samples individual patches along its transect. Flying repeated transects is necessary to achieve a meaningful sample size of each vegetation class. The second approach aims at observing the effective flux at the flight level (assumed to be above the blending height), where the turbulent mixing has already performed some aggregation. Ideally, these observations would physically cover the whole area in a short period

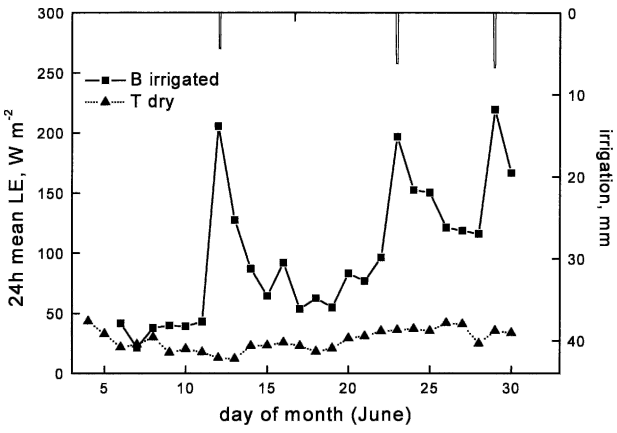

FIG. 8. The 24-h mean latent heat fluxes (W m^{-2}) measured at Barrax (B) flux station located in an irrigated maize site (squares) and at Tomelloso (T) flux station in a vine site (triangles). Irrigation is indicated by the bars at the top of the plot, with the scale on the right side of the plot.

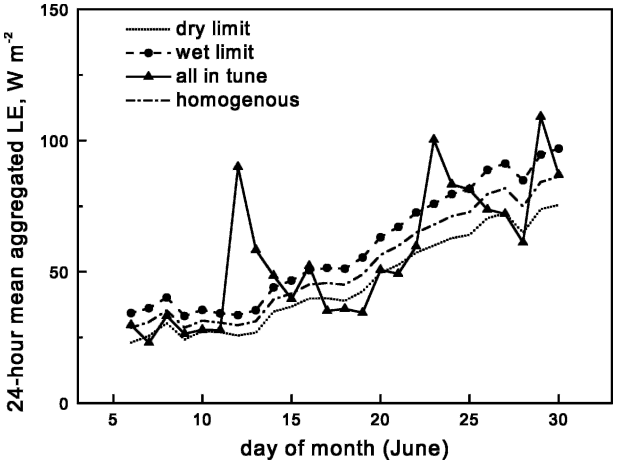

FIG. 9. Area-aggregated 24-h mean surface latent heat flux for an irrigated land area fraction of 40%. For definition of scenarios, see Table 3.

of time. The two approaches are conceptually different and require different types of aircraft.

Given the size and heterogeneity of the EFEDA region, the emphasis was on the second approach. The DLR Falcon is a fast jet aircraft equipped for high-resolution turbulence measurements and is able to cover a large sample of the area in 1 h. Flight legs in the lower ABL (0.07–0.2z_i, where z_i is ML depth) from 7 days are used here. Each flight has two to five legs of 60–105-km length in the given altitude range. The area-averaged flux at flight level is derived through arithmetic averaging of leg mean fluxes.

The use of flux aircraft in heterogeneous terrain often presents the challenge of finding a compromise between turbulence sampling needs and stationarity requirements on a case-to-case basis. Potential errors arise from five fundamental sources, of which the first (instrumental accuracy) is not critical at all (Michels and Jochum 1995). The next two are related to inadequate sampling of turbulent eddies, either by missing the dominant wavelengths or by having too small a sample. These are the systematic and random errors, respectively. They were estimated here from the equations of Mann and Lenschow (1994). Because of the long flight legs, each error is below 15%–20% for heat flux and below 20%–24% for latent flux. The more restricting error source in this case is nonstationarity (Vickers and Mahrt 1997), where homogeneous patches are smaller than sampling criteria would allow. However, these records contain valuable information for the purpose of this work, which was made available by careful visual and analytical inspection of each time series and by compositing whenever possible.

Obtaining the surface fluxes from flight-level fluxes involves some method to account for the low-level flux divergence. Several approaches have been proposed and used (e.g., Betts et al. 1992; Jochum 1993a; Grunwald et al. 1998; Bange et al. 2002). Here the results from a budget analysis (Jochum et al. 2006, manuscript submitted to *J. Hydrometeor.*, hereinafter J06) are used. J06 used a synergistic combination of surface, aircraft, and radiosonde observations in conjunction with the coupled ML model described below. The aircraft dataset includes the four radiation flux components, from which the full radiative divergence was derived. The entrainment parameter was obtained from aircraft measurements at all ABL levels on the basis of the entire midday anticyclonic sample. A simple model relating the surface and inversion-level Bowen ratios was used to derive the latent heat flux divergence.

A four-step procedure is applied to derive the surface energy budget components from aircraft observations. First, the heat flux and net radiation at flight level are calculated from the leg averages. Then, the surface values of heat flux and net radiation are estimated using the low-level flux divergences obtained in the budget analysis (at noon, 0.9 ± 0.05 and 0.12 ± 0.05 K h^{-1}, respectively). Both flux divergences have been shown to vary only slightly across the area (J06). From net radiation R_n, the soil heat flux G is calculated using the mean midday G/R_n relationship ($G/R_n = 0.26 \pm 0.02$) obtained from the surface observations for the noon period. Last, the latent heat flux LE is obtained as the residual of the other terms in the surface energy balance equation ($LE = R_n - H - G$), where H is the sensible heat flux.

The latent heat flux was, of course, measured on the aircraft, and the errors are sufficiently small. However, the budget analysis of J06 shows that the vertical flux divergence changes sign during a short (1–2 h) midday moistening period and that ML moistening is more likely to occur over densely irrigated areas. The energy balance approach circumvents conveniently this problem of flux divergence variations with time and across the area. It also makes the aircraft-derived latent heat fluxes directly comparable to those in the Linder et al. (1996) surface dataset, which were obtained in the same way. An intercomparison of 20-km leg segments flown over the large homogeneous Tomelloso site shows good agreement with flux tower data (Table 4 based on 13 low-level segments from seven flights) and confirms the approach.

b. Regional fluxes from a conservation approach

Radiosondes are able to "see" the regional flow and, thus, offer interesting possibilities to estimate the regional fluxes. Radiosonde-based ML budget methods have been used widely: see the review by Peters-Lidard and Davis (2000) and references therein and, more recent, Cleugh et al. (2004). Many of them follow the line of reasoning of De Bruin (1983) and McNaughton and Spriggs (1986) in developing a set of simplified conservation equations for ML temperature and humidity in a ML slab framework. We use a coupled canopy–ML

TABLE 4. Comparison of surface energy budget components (W m^{-2}) in the Tomelloso area. Sample is 13 flight segments (cut from longer legs) of 20-km length (from 7 flights in 19–29 Jun period). Errors are standard deviations of mean.

	Surface flux observations	Surface flux from aircraft observations
H	252 ± 21	231 ± 37
R_n	458 ± 61	449 ± 12
G	123 ± 18	121 ± 8
LE	84 ± 29	97 ± 39

model here, which consists of two submodels. The ML part is the slab model of Tennekes (1973) with the entrainment formulation of Tennekes and Driedonks (1981). The canopy submodel is based on the (not linearized) governing equations of the Penman–Monteith formula for moisture flux (see de Bruin et al. 2005) and a new parameterization of the soil heat flux as a function of incoming solar radiation. The aerodynamic resistance is stability dependent through application of the Businger–Dyer Monin–Obukhov similarity functions. The surface fluxes of sensible and latent heat, net radiation, and the surface temperature are obtained by solving the nonlinear surface energy budget equation.

Table 5 lists all input parameters required by the model, along with the sets of input data used here for the example of 23 June. Incoming solar radiation, albedo, roughness lengths for momentum and heat, and wind speed were taken from surface observations (Linder et al. 1996). The surface resistance was estimated very roughly as being either "very dry" (500 s m^{-1}) or "very wet" (0). The entrainment factor A was derived as described above. The ML input data were obtained from radiosoundings shortly after sunrise.

The gradients of potential temperature and specific humidity (γ_θ and γ_q) above the ML require special attention whenever they change with time throughout the day. The residual-layer moisture has a layered structure, and so a new humidity gradient is introduced whenever a new moisture layer was reached. This phenomenon was observed regularly in the EFEDA region (Michels and Jochum 1995; Jochum et al. 2004). Compositing these profiles is possible using a multilayer normalization procedure, but this would introduce considerable errors resulting from the observational uncertainties of the individual layer depths.

The model was run for 5 days (where at least four radiosoundings were available over the day). Its validation and calibration for the Tomelloso and Barrax subareas on 23 June (including locally adjusted parameter aggregation rules) confirm that the model is a suitable tool for diagnostic studies at the EFEDA sites.

Comparison with SEB observations at Tomelloso (Fig. 10) shows good agreement of all SEB components except for the afternoon latent heat flux. This high bias is probably because of the observed increase in conductance with the specific humidity deficit, which itself increases over the day (van den Hurk 1996). This mechanism has not yet been incorporated in the model.

The comparison for the Barrax site is different. Because the Barrax area consists of a statistically heterogeneous mixture of irrigated and nonirrigated patches (Fig. 1), the ML is not in equilibrium with any single patch, but rather with the effective properties of all of the patches. The radiosoundings will "see" the ML above the blending height only. Consequently, a column-type comparison for the individual vegetation classes is not possible here.

Therefore, effective surface parameters (last column of Table 5) were derived from experimental calibration, following the set of simple parameter aggregation rules recommended by Shuttleworth (1993). Wind speed, albedo, and incoming solar radiation are averaged linearly. The roughness lengths are treated after Wood and Mason (1991). Effective surface resistances are obtained from linearly averaging the corresponding conductances. All averages are weighted according to the area fraction of each vegetation class, which has been calibrated as 25% irrigated and 75% dry for this exercise. The measure of success was the agreement of the modeled "Barrax aggregate" ML with the observed.

TABLE 5. Input parameters for coupled canopy–mixed layer model (23 Jun); γ_θ and γ_q are the gradients of potential temperature and specific humidity above the ML.

Site	Tomelloso	Barrax aggregate
Wind speed (m s^{-1})	2.2	2.9
Albedo	0.28	0.21
Roughness length z_0 (m)	0.04	0.022
Roughness length for heat z_{0h} (m)	0.004	0.0022
Stomatal resistance r_s (s m^{-1})	500	375
Entrainment factor	0.3	0.2
Initial sounding time	0710	0800
Initial ML depth (m)	350	400
Initial θ (ML) (K)	300	299
Initial q (ML) (g kg^{-1})	6.3	7.3
Jump θ (K)	4	7
Jump q (g kg^{-1})	−2.1	−2
γ_θ (K m^{-1})	0.0025; 0.001 after 1200 UTC	0.001
γ_q (g kg^{-1} m^{-1})	0.000 11; 0.002 after 1030 UTC; −0.001 after 1200 UTC; −0.0013 after 1330 UTC	−0.0005; 0.005 after 1030 UTC; 0 after 1120 UTC; −0.000 15 after 1200 UTC

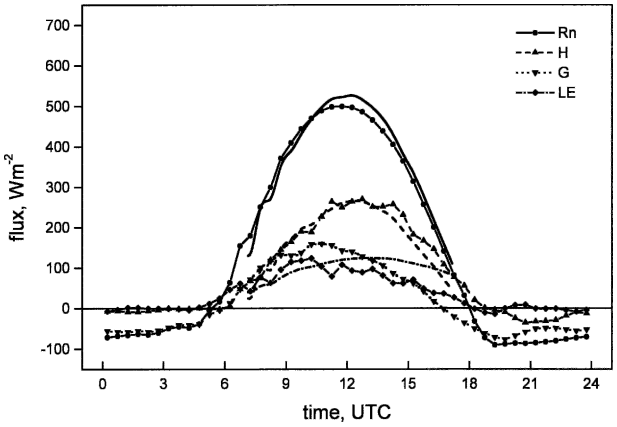

FIG. 10. Comparison of surface energy budget terms from observations (lines with symbols) and coupled canopy–ML model (lines with no symbols) at Tomelloso on 23 Jun 1991.

The model ML depth is very close to that observed (Fig. 11) at both sites. The modeled ML temperature (not shown) at Barrax is as well, while at Tomelloso it remains below the observed ML average. This might be an indication of significant radiative warming, which was indeed found from airborne radiative flux observations (J06). The ML specific humidity (not shown) is reproduced well within the range of observational uncertainty.

6. Synthesis and comparison of grid-scale fluxes

The objective of this work is to obtain grid-scale fluxes for a range of areas. Table 6 lists the areas of interest. One is obviously the whole EFEDA region. The others are subareas defined according to the grid cells of the numerical models. These subareas were selected to differ by size and geographical location and, therefore, by fractions of land use classes. The High-Resolution Limited-Area Model (HIRLAM) serves here as an example of a numerical weather prediction model that has been evaluated for the EFEDA region (Jochum et al. 2004). Both the standard resolution of the operational version (0.5°) and the current high-resolution version (0.2°) are considered (H05B and H02B in Table 6). An experimental very high resolution grid element of 0.05° (E05B) is also used. Figure 12 shows a diurnal cycle example (23 June) of fluxes for these grid cells. Figure 13 shows a 3-day sequence (part of the sequence in Fig. 6).

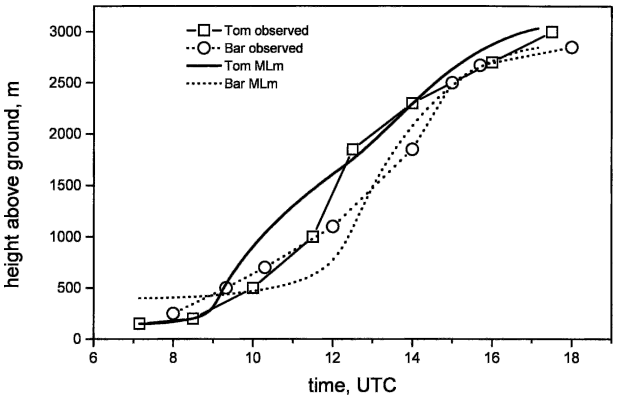

FIG. 11. Comparison of ML depth at Tomelloso (solid lines) and Barrax (dotted lines) on 23 Jun. Observations (lines with squares and circles) are taken from Michels and Jochum (1995). Lines with no symbols are from coupled canopy–ML model (MLm).

Following the discussion in section 3, it is clear that the aggregated fluxes depend on the fraction of irrigated land and, thus, on the size and location of the area. Mahrt et al. (2001) observe a similar phenomenon in the case of BOREAS, where the area aggregates depend on the fraction of coniferous versus deciduous forest. The influence of irrigated land, however, is much stronger.

Grunwald et al. (1996) recognized the importance of the irrigated fields in their Barrax 10 km × 10 km area average. They use the 7-day history of a moisture indicator (based on the fraction of evaporation and global radiation) to derive area-averaged fluxes on a single day. Here, the interest is on obtaining a time series of regional fluxes for the whole month of June. Therefore, a simpler approach has been developed (sections 3 and 4). It was shown that the latent heat flux measured at the Barrax-irrigated flux tower (located in a maize center pivot) is a suitable observational basis for flux aggregation, provided a normalization is applied that scales the daily observed latent heat flux to the daily ET_c. With this adjustment, the flux tower ET comes very close to the probable behavior of irrigation farmers and retains the diurnal cycle dynamics. Figure 13 demonstrates the effect of the normalization for a 3-day sequence (22–24 June) and for area E05B. The latent heat flux on 22 June (day before irrigation night, close to "dry limit") is raised by the scaling, while on 23 June (peak day after irrigation) it is lowered. The slow increase of the midday peak fluxes over the 3 days reflects only the increasing ET_c (see Fig. 4), but not the individual field irrigation-on/-off dynamics. Another adjustment to the regional flux time series needs to be made in order to account for the presence of irrigated crops other than maize.

a. Comparison of regional flux estimates

Grid-scale fluxes from weighted surface observations are now compared with results from other approaches based on intensive observation periods (airborne flux observations and regional fluxes from a radiosonde–ML model-based conservation approach). Additional runs of the coupled canopy–ML slab model were made

TABLE 6. Fractional area covered in 1991 by each vegetation class in the EFEDA region and in the corresponding model grid elements within and around that region (%). H05B (H02B) denotes the HIRLAM grid cell around Barrax at 0.5° (0.2°) resolution; H02T is analogous for Tomelloso; E05B is an experimental very high resolution grid cell at 0.05° resolution.

	EFEDA	H05B	H02B	E05B	H02T
Lat	38.92°–40.08°N	39.0°–39.5°N	39.0°–39.2°N	39.10°–39.15°N	39.0°–39.5°N
Lon	2.18°–3.18°W	2.0°–2.5°W	2.0°–2.2°W	2.10°–2.15°W	2.0°–2.5°W
Area (km^2)	8000	2976	475	29.7	475
SUM-dry	45	28	46	5	97
BARE, SPR-dry, SPR-irrig	45	63	42	55	3
SUM-irrig	5	7	12	40	0
NAT, FOR	5	2	0	0	0

with a new set of input parameters aggregated for the whole area, following the same approach as in section 5. The flux uncertainties are of the same order of magnitude as that of aircraft flux estimates (section 2). The results for 23 June are presented here; other days are similar. Figure 12 shows the area-aggregated sensible and latent heat fluxes for selected areas (Table 6). The difference between areal fluxes is largest in the latent flux, where a range of 123–280 W m^{-2} is found in midday maxima and a phase shift of the occurrence of the maximum ranges from 1000 to 1300 UTC. The overall EFEDA region and the 0.5° grid cells behave similarly to the "dry" grid cells, but at the level of 0.2° resolution (19 km × 24 km); the character of the grid-scale fluxes is rather "wet" in the vicinity of Barrax. With smaller grid cells, zooming in on the irrigated zone (E05B), this effect increases. The sensible heat flux varies less. The whole area aggregate closely resembles the dry cells, with a midday peak of about 260 W m^{-2}, whereas the wettest grid cell reaches a maximum of 210 W m^{-2}.

The aircraft estimate of surface sensible heat flux at noon is within the range of the wet cells and thus remains below the whole area surface aggregate, but the uncertainty ranges overlap. The aircraft estimate of surface latent heat flux is slightly higher than that of the weighted surface average, but is well within the range of uncertainty. The "airborne surface flux" uncertainty is composed of four factors. Direct flux errors and the range of spatial variability at flight level can be assessed from the data (about 24% for sensible heat flux and 34% for latent heat flux, see section 2). Errors in the low-level flux divergence and ML depth (which propagate into the normalized height z/z_i) are estimated to be roughly of the same order. The ML depth derived from aircraft or radiosonde (single-point profile) measurements are in error mainly because of the undulating nature of the ML top. Uncertainty in ML depth is still large at noon, because the ML reaches its full depth late in the afternoon (Michels and Jochum 1995).

The grid-scale flux comparison of net radiation (not shown) gives a range of noon peak values from 500 to 600 W m^{-2}, while the soil heat flux (not shown) gives visibly different values only during the afternoon transition. The spread of net radiation is explained by the behavior of albedo and surface temperature (not shown). Results from the comparison of other days are similar; they do not indicate any systematic bias in the tower-based flux aggregate and thus there is no need to make any adjustments here.

b. Adjustment for heterogeneous cloud cover

Small cumulus clouds were observed in the area on several days and some diurnal cycle data show their effects on the SEB. Using these data directly in the flux aggregation algorithm would introduce a bias in the regional flux. Therefore, a simple procedure was developed to adjust the grid-scale aggregate fluxes for heterogeneous cloud cover. First, a "cloud mask" is applied, using the incoming solar radiation time series, which then, along with net radiation, is reconstructed by means of sine-interpolated curves. The maximum value at local noon is used from the station if it is cloud free, or else it is interpolated from adjacent days. The remaining terms of the SEB are then adjusted accordingly. In a second step, the cloud cover percentage on each day (assumed the same for each vegetation class) is determined from HIRLAM output, and is validated on some days with observations and/or Landsat data. Last, the weights in Eq. (1) are adjusted accordingly.

c. Practical considerations

The steps to follow in the generation of the consolidated dataset of grid-scale fluxes are summarized here. They refer to the EFEDA region and observations, but can easily be adjusted to similar (semi) arid environments. In each case, the irrigation practice in the area and year/season needs to be taken into account (e.g., cropping patterns, multiple cropping on the same fields, deficit irrigation).

1) Take the land use classification of Calera Belmonte (2000) or a similar product (that differentiates ac-

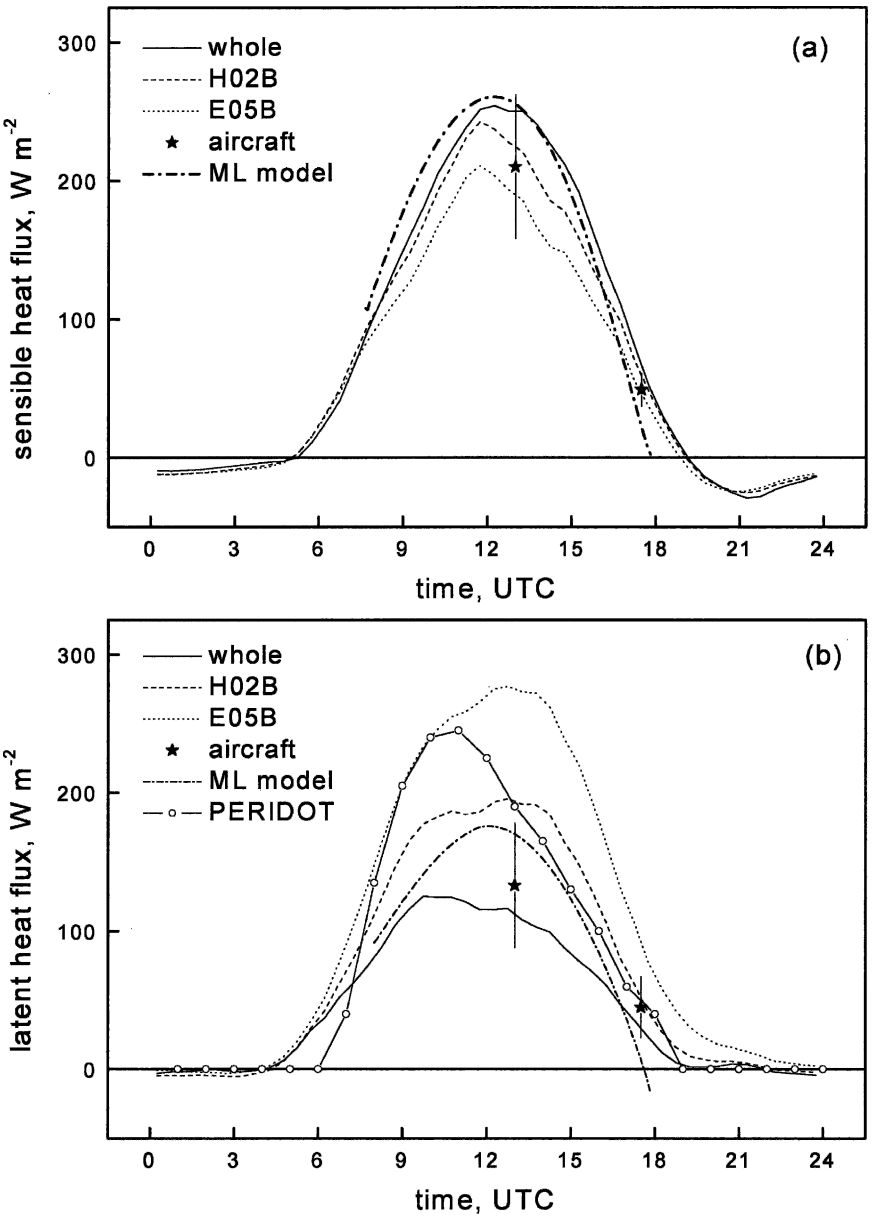

FIG. 12. Area-aggregated (a) sensible and (b) latent heat flux for the whole EFEDA region (solid line) and for different subareas (see Table 6) on 23 Jun 1991. The asterisk with error bars represents the airborne estimate. Dash–dotted line gives radiosonde–ML slab model results. The open circles in (b) represent a selection of the mesoscale model results of Noilhan (1996).

cording to phenological cycles, which means that it has to be multitemporal). Note that these classifications vary from year to year (because of varying cropping patterns).

2) Define the major vegetation classes (based on K_c and ET_c curves) and get tower observations of SEB in each. Get areal fractions of the major classes from the classification.
3) For flux tower(s) in irrigated fields, get daily ET_c data and adjust the measured fluxes by scaling the 24-h mean latent heat flux with daily ET_c.
4) Adjust measured SEB_s according to the presence of other crops in the same class, when necessary.
5) Adjust all SEBs for heterogeneous cloud cover when needed.

The area-aggregated fluxes can now be calculated from Eq. (1) for each area of interest.

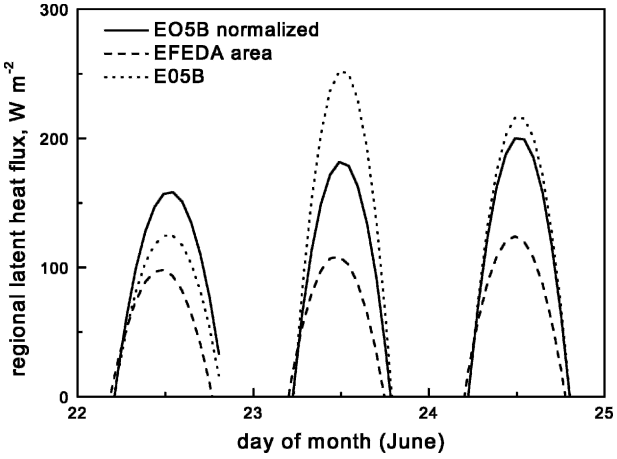

FIG. 13. Three-day sequence of half-hourly aggregated latent heat flux for whole EFEDA region (dashed line) and grid cell E05B without (dotted line) and with (solid line) normalization.

d. Perspective

One purpose of the observational grid-scale flux time series is the validation of surface and ABL schemes in numerical models. We show here an example for a mesoscale model that was extensively validated with EFEDA data. Noilhan et al. (1997) used the Météo France hydrostatic model "PÉRIDOT" for aggregation studies at a grid size of 10 km. Noilhan (1996) showed that parameter aggregation results are practically equal to the flux-aggregated values in this case. Figure 12 includes his results and shows that all daytime model fluxes are consistently higher than the observational surface aggregate. This is surprising, because the model's land surface scheme [Interactions between Soil, Biosphere, and Atmosphere (ISBA); Noilhan and Planton 1989] was successfully validated with EFEDA surface observations previously (Noilhan 1996). A simple explanation would be that their land use classification might be biased toward "green" crops (with high fractional ground cover). Jochum et al. (2004) find a similar bias in HIRLAM (which also uses the ISBA surface scheme).

EFEDA was one of the earliest land surface experiments, so many recommendations on observational strategy have already been put in practice in later observational studies of similar objectives and magnitude (e.g., the coverage of seasonal or longer time scales). We would add here and stress again (Jochum et al. 2004) the importance of dense and frequent atmospheric humidity profiling in areas with similarly large heterogeneity of atmospheric moisture fields.

Remote sensing was not explicitly addressed here, although it offers interesting approaches to estimate pixel-wise SEB (e.g., Bastiaanssen et al. 1997; Gao et al. 1998). Both ET_0 and ET_c can reliably be estimated from satellite image data (Schüttemeyer 2005; Calera Belmonte et al. 2005); thus, the irrigation patterns can be quantified increasingly better. High-resolution satellite-derived ET_c has recently been incorporated in operational irrigation scheduling by IAS (Jochum et al. 2005). These are prominent examples of the wealth of data available in the water management sector, which are of great interest for flux aggregation purposes, but also in general for the land surface, weather prediction, and climate communities. A link between these communities would be beneficial for both.

7. Conclusions

This paper studies aggregation and regional fluxes in the semiarid EFEDA environment. Area-averaged fluxes for a range of areas, including the whole EFEDA region (50–100-km scale) and four HIRLAM grid cells (10–50-km scale), are derived, and several approaches are discussed on the grounds of the available data. Weighted averages of surface observations are the only possible choice for the practical purpose of providing monthly or seasonal time series of aggregated fluxes. Intensive short-term observations (e.g., from aircraft and radiosondes) help to identify potentially required adjustments to these values (for strata, processes, and/or scales not covered).

The weighted surface observations were compared with regional fluxes from aircraft and a radiosonde-ML-model-based conservation approach. The results of the different methods agree within the range of uncertainty and do not provide evidence of any need for adjustments to the flux tower averages.

The main lesson from this aggregation exercise concerns the role of irrigation. First, this study quantifies the uncertainties in the space–time pattern and its effects on aggregated surface fluxes for the first time on the grounds of observational data. It corroborates model-based findings of Adegoke et al. (2003), de Rosnay et al. (2003), Zaitchik et al. (2005), and Haddeland et al. (2006). Second, it demonstrates practical ways to accomplish the parameterization of irrigation in flux aggregation schemes, by identifying the key data along with their possible sources and by defining a practical implementation procedure.

The area-aggregated fluxes from weighted surface observations are highly sensitive to the fraction of irrigated land, which highlights the need of its correct iden-

tification in the land use classification and in the delineation of the area. The skill in aggregating surface fluxes in this type of area consists of correctly estimating the percentage of actually irrigated land and quantifying and parameterizing the irrigation practices of the area. The land use classification of Calera Belmonte (2000) provides the appropriate differentiation according to the crop phenological cycles. It is used here in conjunction with the observed surface fluxes from the vegetation class–averaged dataset of Linder et al. (1996). Irrigation scheduling in the area is based on weekly cycles. In a statistical sense, most irrigated fields are maintained close to ET_c (Montoro et al. 2004). It follows from a scenario approach that without entering in details of the irrigation history of each field, a good parameterization is obtained from scaling the irrigated flux station data (located in a maize field) with daily ET_c.

In conclusion, surface flux aggregation in (semi) arid environments with major agricultural activity cannot be done without knowing the irrigation practices in vigor at a given moment in a given area. These have evolved over time and continue evolving, given the ever-increasing scarcity of water resources on one hand and the emerging knowledge of factors influencing water productivity on the other. For example, in the Barrax area, farmers used to irrigate approximately according to ET_c (as recommended by the Food and Agriculture Organisation; Allen et al. 1998), with a slight tendency to overirrigate. With time, and supported by a strong local Irrigation Advisory Service (Montoro et al. 2004), they have been using less water and deficit irrigation has become fairly common.

Many data on actual irrigation practices are available, although not automatically to the land surface and climate community. For this purpose, the link needs to be established with the operational water management sector, where comprehensive datasets on water availability and the use of irrigated crops are generated at increasingly high space–time resolution (Jochum et al. 2005; Calera Belmonte et al. 2005). This paper intends to raise awareness not only of the importance but also of the feasibility of integrating irrigation practice data in flux aggregation and numerical weather prediction and climate modeling.

Acknowledgments. All EFEDA participants have contributed to providing a complete and high-quality dataset. In particular, we thank Joël Noilhan for providing us with the surface dataset of Linder et al. (1996), Pierre Bessemoulin and Norbert Kalthoff for making available their radiosonde and surface flux data, and last, but not least, Hans-Jürgen Bolle for coordinating this large field effort. Thanks also are given to José González for sharing his crop coefficient data and to Bart van den Hurk for comments on an earlier manuscript version. The detailed comments of one of the reviewers were very helpful. The EFEDA 1991 field phase was partly supported by the European Commission under its Environment Program (Grant EV5V-CT93-0271).

REFERENCES

Adegoke, J. O., R. R. Pielke Sr., J. Eastman, R. Mahmood, and K. G. Hubbard, 2003: Impact of irrigation on midsummer fluxes and temperature under dry synoptic conditions: A regional atmospheric model study of the U.S. High Plains. *Mon. Wea. Rev.,* **131,** 556–564.

Allen, R. A., L. S. Pereira, D. Raes, and M. Smith, 1998: Crop evapotranspiration: Guidelines for computing crop water requirements. FAO Irrigation and Drainage Paper 56, 300 pp.

André, J. C., and Coauthors, 1988: HAPEX-MOBILHY: First results from the special observing period. *Ann. Geophys.,* **6,** 477–492.

——, P. Bougeault, and J.-P. Goutorbe, 1990: Regional estimates of heat and evaporation fluxes over non-homogeneous terrain; examples from the HAPEX-MOBILHY program. *Bound.-Layer Meteor.,* **50,** 77–108.

Bange, J., F. Beyrich, and D. A. M. Engelbart, 2002: Airborne measurements of turbulent fluxes during LITFASS-98: Comparison with ground measurements and remote sensing in a case study. *Theor. Appl. Climatol.,* **73,** 35–51.

Bastiaanssen, W. G. M., H. Pelgrum, P. Droogers, H. A. R. de Bruin, and M. Menenti, 1997: Area-average estimates of evaporation, wetness indicators and top soil moisture during two golden days in EFEDA. *Agric. For. Meteor.,* **87,** 119–137.

Beljaars, A. C. M., and A. A. M. Holtslag, 1991: Flux parameterization over land surfaces for atmospheric models. *J. Appl. Meteor.,* **30,** 327–341.

Betts, A. K., R. L. Desjardins, J. I. McPherson, and R. D. Kelly, 1992: Budget analysis of the boundary layer grid flights during FIFE 1987. *J. Geophys. Res.,* **97,** 18 533–18 546.

Beyrich, F., H. J. Herzog, and J. Neisser, 2002: The LITFASS project of DWD and the LITFASS-98 experiment: The project strategy and the experimental setup. *Theor. Appl. Climatol.,* **73,** 35–51.

Bolle, H.-J., and Coauthors, 1993: EFEDA: European Field Experiment in a Desertification-threatened Area. *Ann. Geophys.,* **11,** 173–189.

Calera Belmonte, A., 2000: Seguimiento mediante teledetección de la cubierta vegetal de los cultivos de secano y su relación con variables climáticas en Castilla La Mancha (Remote sensing–based monitoring of rainfed crops in Castilla-La Mancha). Ph.D. thesis, University of Valencia, 315 pp. [Available from A. Calera, IDR, E-02071 Albacete, Spain.]

——, A. M. Jochum, A. Cuesta García, A. Montoro Rodríguez, and P. López Fuster, 2005: Irrigation management from space: Towards user-friendly products. *Irrig. Drain. Syst.,* **19,** 337–353.

Cleugh, H. A., M. R. Raupach, P. R. Briggs, and P. A. Coppin, 2004: Regional-scale heat and water vapour fluxes in an agricultural landscape: An evaluation of CBL budget methods at OASIS. *Bound.-Layer Meteor.,* **110,** 99–137.

de Bruin, H. A. R., 1983: A model for the Priestley-Taylor α. *J. Climate Appl. Meteor.,* **22,** 572–578.

——, and Coauthors, 1993: Surface fluxes measured during EFEDA. EFEDA Final Report, H. J. Bolle and B. Streckenbach, Eds., Institut für Meteorologie, Freie Universität Berlin, 141–227.

——, O. K. Hartogensis, R. G. Allen, and J. W. J. L. Kramer, 2005: Note on the Regional Advection Perturbations in an Irrigated Desert (RAPID) experiment. *Theor. Appl. Climatol.,* **80,** 143–152.

de Rosnay, P., J. Polcher, K. Laval, and M. Sabre, 2003: Integrated parameterization of irrigation in the land surface model ORCHIDEE. Validation over Indian peninsula. *Geophys. Res. Lett.,* **30,** 1986, doi:10.1029/2003GL018024.

Gao, W., R. L. Coulter, B. M. Lesht, J. Qiu, and M. L. Wesely, 1998: Estimating clear-sky regional surface fluxes in the Southern Great Plains Atmospheric Radiation Measurement site with ground measurements and satellite observations. *J. Appl. Meteor.,* **37,** 5–22.

González-Piqueras, J., 2006: Evapotranspiración de la cubierta vegetal mediante la determinación del coeficiente de cultivo por teledetección. Extensión a escala regional: Acuífero 08.29 Mancha Oriental (Canopy evapotranspiration from remote sensing of crop coefficient: Extension to the regional scale and application to the aquifer 08.29 Mancha Oriental). Ph.D. thesis, Universitat de València, 240 pp. [Available from J. González, IDR, E-02071 Albacete, Spain.]

Gottschalk, L., and Coauthors, 1999: Scale aggregation—Comparison of flux estimates from NOPEX. *Agric. For. Meteor.,* **98–99,** 103–119.

Grunwald, J., N. Kalthoff, U. Corsmeier, and F. Fiedler, 1996: Comparison of areally averaged turbulent fluxes over nonhomogeneous terrain. *Bound.-Layer Meteor.,* **77,** 105–134.

——, ——, F. Fiedler, and U. Corsmeier, 1998: Application of different flight strategies to determine areally averaged turbulent fluxes. *Contrib. Atmos. Phys.,* **71,** 283–302.

Haddeland, I., D. P. Lettenmaier, and T. Skaugen, 2006: Effects of irrigation on the water and energy balances of the Colorado and Mekong River basins. *J. Hydrol.,* in press.

Halldin, S., S. E. Gryning, L. Gottschalk, A. M. Jochum, L.-C. Lundin, and A. A. van de Griend, 1999: Energy, water and carbon exchange in a boreal forest landscape—NOPEX experiences. *Agric. For. Meteor.,* **98–99,** 5–29.

Holtslag, A. A. M., and M. Ek, 1996: Simulation of surface fluxes and boundary layer development over the pine forest in HAPEX-MOBILHY. *J. Appl. Meteor.,* **35,** 202–213.

Jochum, A. M., 1993a: Estimation of area-averaged fluxes from aircraft measurements using different observational techniques. *Proc. Eighth Symp. on Meteorological Observations and Instrumentation,* Anaheim, CA, Amer. Meteor. Soc., 469–472.

——, 1993b: Evaporation and energy fluxes during EFEDA: Horizontal variability and area averaging. *IAHS Publ.,* **212,** 373–380.

——, P. Kabat, and R. Hutjes, 2000: The role of remote sensing in land-surface experiments within BAHC and ISLSCP. *Observing Land from Space: Science, Customers and Technology,* M. Verstraete, M. Menenti, and J. Peltoniemi, Eds., Kluwer Academic, 91–103.

——, E. Rodríguez Camino, H. A. R. de Bruin, and A. A. M. Holtslag, 2004: Performance of HIRLAM in a semi-arid heterogeneous region: Evaluation of the land-surface and boundary layer description using EFEDA observations. *Mon. Wea. Rev.,* **132,** 2745–2760.

——, A. Calera Belmonte, A. Montoro Rodríguez, P. López Fuster, and A. Cuesta García, 2005: Servicio de Asesoramiento de Riegos Asistido por Satélite: Operación en tiempo real y evaluación por usuarios (Space-assisted Irrigation Advisory Service: Real-time operations and evaluation with users). *Proc. XXIII Congreso Nacional de Riegos,* Elche, Spain, Asociación Española de Riegos y Drenaje, 58–59.

Leuning, R., and Coauthors, 2004: Spatial and temporal variations in fluxes of energy, water vapour and carbon dioxide during OASIS 1994 and 1995. *Bound.-Layer Meteor.,* **110,** 3–38.

Linder, W., J. Noilhan, M. Berger, K. Bluemel, E. Blyth, and G. Boulet, 1996: Intercomparison of surface schemes using EFEDA flux data. Météo France CNRM Rep. 39, 86 pp.

Mahrt, L., D. Vickers, J. Sun, and J. H. McCaughey, 2001: Calculation of area-averaged fluxes: Application to BOREAS. *J. Appl. Meteor.,* **40,** 915–920.

Mann, J., and D. H. Lenschow, 1994: Errors in airborne flux measurements. *J. Geophys. Res.,* **99,** 14 519–14 526.

Martínez, C., and A. Calera, 2001: Irrigated crop area estimation from thematic map using Landsat TM imagery in La Mancha (Spain). *Photogram. Eng. Remote Sens.,* **67,** 1177–1184.

McNaughton, K. G., and T. W. Spriggs, 1986: A mixed-layer model for regional evaporation. *Bound.-Layer Meteor.,* **34,** 243–262.

Michaud, J. D., and W. J. Shuttleworth, 1997: Executive summary of the Tucson Aggregation Workshop. *J. Hydrol.,* **190,** 176–181.

Michels, B. I., and A. M. Jochum, 1995: Heat and moisture flux profiles in a region with inhomogeneous surface evaporation. *J. Hydrol.,* **166,** 383–407.

Montoro, A., R. López Urrea, and P. López Fuster, 2004: El Servicio de Asesoramiento de Riegos de Albacete: Dieciseis años de experiencia (The Irrigation Advisory Service of Albacete: Sixteen years of experience). *Proc. XXII Congreso Nacional de Riegos,* Logroño, Spain, Asociación Española de Riegos y Drenaje, 75–76.

Noilhan, J., 1996: Desertification processes in the Mediterranean area and their interlinks with global climate: Surface processes and atmospheric modelling. Final Report of the EFEDA Group 6, EU Contract EV5V-CT93-0269, 165 pp.

——, and S. Planton, 1989: A simple parameterization of land surface processes for meteorological models. *Mon. Wea. Rev.,* **117,** 536–549.

——, P. Lacarrère, A. J. Dolman, and E. M. Blyth, 1997: Defining area-average parameters in meteorological models for land surface with mesoscale heterogeneity. *J. Hydrol.,* **190,** 302–316.

Pelgrum, H., and W. G. M. Bastiaanssen, 1996: An intercomparison of techniques to determine the area-averaged latent heat flux from individual in situ observations: A remote sensing approach using the EFEDA data. *Water Resour. Res.,* **32,** 2775–2786.

Peters-Lidard, C., and L. H. Davis, 2000: Regional flux estimation in a convective boundary layer using a conservation approach. *J. Hydrometeor.,* **1,** 170–182.

Schmid, H. P., 1994: Source areas for scalars and scalar fluxes. *Bound.-Layer Meteor.,* **67,** 293–318.

Schüttemeyer, D., 2005: The surface energy balance over drying semi-arid terrain in West Africa. Ph.D. thesis, Wageningen University, 154 pp.

Sellers, P. J., and Coauthors, 1997: BOREAS in 1997: Experiment overview, scientific results and future directions. *J. Geophys. Res.,* **102,** 28 731–28 769.

Shuttleworth, W. J., 1993: The soil-vegetation-atmosphere interface. *Energy and Water Cycles in the Climate System*, E. Raschke and D. Jakob, Eds., Proc. NATO ASI, Vol. 15, Springer-Verlag, 323–364.

Tennekes, H., 1973: A model for the dynamics of the inversion above a convective boundary layer. *J. Atmos. Sci.,* **30,** 558–567.

——, and A. G. M. Driedonks, 1981: Basic entrainment equations for the atmospheric boundary layer. *Bound.-Layer Meteor.,* **20,** 515–531.

van den Hurk, B. J. J. M., 1996: Sparse canopy parameterizations for meteorological models. Ph.D. thesis, Wageningen University, 272 pp.

Vickers, D., and L. Mahrt, 1997: Quality control and flux sampling problems for tower and aircraft data. *J. Atmos. Oceanic Technol.,* **14,** 512–526.

Wood, N., and P. J. Mason, 1991: The influence of static stability on the effective roughness for momentum and heat transfer. *Quart. J. Roy. Meteor. Soc.,* **117,** 1025–1056.

Zaitchik, B. F., J. Evans, and R. B. Smith, 2005: MODIS-derived boundary conditions for a mesoscale climate model: Application to irrigated agriculture in the Euphrates Basin. *Mon. Wea. Rev.,* **133,** 1727–1743.